

# FUSION REACTIVITY CHARACTERIZATION OF A SPHERICALLY CONVERGENT ION FOCUS

T.A. THORSON, R.D. DURST, R.J. FONCK, A.C. SONTAG  
University of Wisconsin-Madison,  
Madison, Wisconsin,  
United States of America

**ABSTRACT.** The deuterium–deuterium (D–D) fusion reaction rate in a spherically convergent ion focus is observed to significantly exceed the rate predicted by a collisionless flow model. However, a careful consideration of ion–neutral collisions and the trapped neutral density in the cathode account for the extra reactivity without invoking anomalous ion trapping in the converged core region. This conclusion is supported by proton collimation measurements, which indicate that the bulk of the observed reactivity originates outside the core region. In addition, a classical flow model, where charge exchange collisional effects on the ion and fast neutral distributions are included, provides fusion rate estimates that are quantitatively consistent with the observed D–D fusion neutron production rate.

## 1. INTRODUCTION

Spherically convergent ion focus (SCIF) is an electrostatic confinement concept where ions are accelerated to fusion relevant energies towards the origin of a transparent spherical cathode. The ions then recirculate through the cathode, and fusion reactions occur between the counterflowing ions or between the ions and the background neutral particles. Some noteworthy features of these devices are that energetic ions are easily obtained, the fuel inventory is lower than that for conventional particle sources and the ions may be tuned in energy to the peak cross-section for different fusion reactions. These devices may be well suited for a variety of particle source applications including neutron activation or scattering analysis, oil well logging and detection of chemical weapons or explosives [1–3]. It has even been suggested [4–8] (and refuted [9, 10]) that more advanced but related ion focus concepts could be considered as alternate concepts for power production.

Early studies of this type were performed by Lavrent'ev [11], followed by the first fusion reactivity experiments carried out by Hirsch [12], using high energy ion guns as a source of ions. The fusion produced neutron rates measured in Hirsch's experiments (approaching  $10^{10}$  n/s in deuterium–tritium (D–T)) were much higher than those predicted using an estimate with an ideal, collisionless model. Recently, much work has been performed with devices using a transparent grid as the cathode and either a diffuse edge plasma or a spherical glow discharge as the ion source [1–5]. Reactivity

measurements performed in these gridded sources used by Miley et al., and those discussed herein, are below those of Hirsch, presumably owing to the use of discrete, directed ion guns in Hirsch's work at energies considerably higher than those used in spherical grid experiments (i.e. 75 keV/amu versus 25 keV/amu). However, the gridded systems also often show more fusion production (as much as a factor of 5 higher) than the ideal, collisionless expectations. To some degree, it is this appearance of an unexplained, anomalously high fusion reactivity in these devices that has maintained the interest in them.

In general, the basic sources of fusion reactivity observed in low power experiments to date remain experimentally unexplored and hence unexplained. Therefore, it has been difficult to judge the viability of these devices for the proposed applications.

To provide a better framework for addressing some of these issues, we report here results of new experiments aimed at determining the source of the D–D fusion reactivity for a gridded SCIF device. We also develop a fluid flow model with charge exchange production of energetic neutrals to provide a reasonably quantitative accounting for the measured reactivity. Although the original ion gun experiments achieved higher fusion production, we concentrate here on studying the reactivity in a simpler (and lower cost) spherical grid system with an extended plasma ion source, as these devices also appear to give excess reactivity, are considered for near term applications and are often used in the search for any anomalous enhancement of the reactivity [1–5].

The next section discusses the various sources of reactivity in a gridded SCIF device, with prescriptions for quantitatively estimating each source term. This is followed by a description of the WISCIF (Wisconsin SCIF) experimental apparatus. The fourth section of this article reports the results of the D–D fusion production rate measurements under a variety of experimental conditions.

Finally, these measurements are shown to be consistent with a classical ion flow model that includes charge exchange to produce fast neutral atoms, which can then fuse with the background neutral gas. In addition, the contribution due to the trapped neutral density at the cathode surface is found to be non-negligible at the lowest neutral gas pressures.

## 2. SOURCES OF REACTIVITY IN A SCIF DEVICE

The fusion reactivity of a spherical electrostatic trap results from a variety of sources, including beam–beam, beam–background, beam–cathode and fast-neutral–background collisions. Here, beam indicates the primary fast ions accelerated by the spherical potential well, background indicates the cold neutral fill gas atoms or molecules, cathode indicates the trapped fuel density in the solid cathode and fast neutral indicates energetic neutral atoms produced by charge exchange reactions between the beam ions and the background gas. Assuming spherical symmetry, the system fusion production rate,  $R_{\text{fus}}$ , is given by

$$R_{\text{fus}} = 4\pi \int_0^\rho r^2 dr n_f(r, v) \left( n_0 \overline{\sigma_f v(r)_0} + \frac{n_f(r, v)}{4} \overline{\sigma_f v(r)_f} \right) + R_{\text{fus,cat}} \quad (1)$$

where  $\rho$  is the radius of the reaction volume,  $n_f(r, v)$  is the fast particle density (ions or fast neutrals),  $n_0$  is the neutral fuel gas density,  $\sigma_f v(r)$  is the fusion reaction rate (which must be averaged over the appropriate relative velocities of the interacting particles) and  $R_{\text{fus,cat}}$  is the contribution from the particles trapped in the cathode. The first term in the integrand in Eq. (1) refers to reactions that scale linearly with the injected current ( $n_f \propto I$ ), and the second term describes beam–beam interactions, which scale as the injected current squared.

To compare past experimental reactivity measurements [1–5, 12] and results reported herein with Eq. (1), the ion density and velocity distributions

must be known. A model that is typically used as a first estimate for these distributions is one that ignores collisions and assumes a monoenergetic ion distribution, with energy  $E_i = -\Phi(r)$ , the local plasma potential. Since collisions would be expected to degrade rather than enhance the fusion rate, this estimate is optimistic and provides an upper limit for the expected values of  $R_{\text{fus}}$  with classical unperturbed ion flow. In addition, the presence of a virtual anode, formed by the charge buildup in the core due to the convergent ion flow, is ignored to first order. Since any such anode (which has been experimentally observed [13, 14]) will decelerate the beam ions, this assumption also tends to an overestimate of the expected  $R_{\text{fus}}$  in the core region.

Using this collisionless model, ion current conservation ( $I = 4\pi e r^2 n_i v = \text{const}$ ) requires that the radial ion density distribution,  $n_i(r)$ , for a perfectly converging system is given by

$$n_i(r) = n_i(R) \left( \frac{R}{r} \right)^2 \frac{v(R)}{v(r)} = \frac{I}{4\pi e r^2 v(r)} \quad (2)$$

where  $v(r)$  is the ion velocity and  $I$  is the total recirculating ion current. This current is related to the measured cathode current by [14]

$$I = \frac{I_{\text{meas}}}{(1 - \eta^2)(1 + \delta_e)} \quad (3)$$

where  $\eta$  is the effective cathode transparency and  $\delta_e$  is the secondary electron emission coefficient for the cathode material.

Angular momentum, due to finite temperature or asymmetries in the accelerating potential, keeps the density from diverging at  $r = 0$ , and an ion ‘core’ then forms in the vicinity of  $r = 0$ . In the absence of ion trapping, the core ion density for a recirculating ion flow is modelled as a constant value given by [14]

$$n_{\text{ic}} = \frac{\eta I_{\text{meas}}}{(1 - \eta^2)(1 + \delta_e)} \left( \frac{1}{e v_c \pi r_c^2} \right) \quad (4)$$

where  $v_c$  is the velocity of the ions through the core and  $r_c$  is the core radius.

For typical operating parameters in past experiments ( $P \sim 500$  mPa,  $I_{\text{meas}} \sim 20$  mA), Eq. (4) estimates the core ion density to be  $\sim 10^{15}$  m $^{-3}$  (assuming  $\delta_e = 1$ ,  $r_c = 5$  mm,  $\eta = 0.95$  and a core ion energy of 35 kV), which is much less than the neutral gas density ( $\sim 10^{20}$  m $^{-3}$ ). Therefore, the beam–beam interactions ( $\propto n_i^2$ ) should be weak compared with the beam–background reactions ( $\propto n_i n_0$ ).

This expectation is illustrated by estimating the fusion neutron production rate for the WISCIF device

(described below) at these conditions. The core ion density is first calculated from Eq. (4), given  $V_{\text{cat}}$ ,  $I_{\text{meas}}$ ,  $\delta_e$ ,  $\eta$  and  $r_c$ . Outside the cathode, a potential distribution limited by space charge is assumed, and the remaining radial density distribution is then given by the current conservation model (substitute  $r_c$  for  $R$  in Eq. (2)). The fusion reaction rates,  $\sigma_f v(r)$ , are calculated as a function of  $r$  (for beam–beam,  $E_i = -4q\Phi(r)$ , for beam–background,  $E_i = -q\Phi(r)$ ), and the resulting  $n_i(r)$  and  $\sigma_f v(r)$  distributions are substituted into Eq. (1). The integral for the total fusion production rate ( $R_{\text{fus}}$ ) is then determined numerically.

Using this model and applying the typical operating conditions of past experiments to the WISCIF experiment ( $r_{\text{cat}} = 0.05$  m,  $\rho = 0.20$  m), Eq. (1) then calculates the beam–background reaction rate to be more than 4 orders of magnitude higher than the beam–beam rate. In addition, about 85% of the beam–background fusion reactions occur inside the cathode radius (10% in the core region, 75% between  $r_c$  and  $r_{\text{cat}}$ ). The remaining 15% occurs at  $r > r_{\text{cat}}$ . This is in contrast to the beam–beam spatial distribution of fusion production, where about 70% is expected inside the core and 30% between  $r_c$  and  $r_{\text{cat}}$  ( $\ll 1\%$  of the beam–beam contribution is expected to occur for radii greater than  $r_{\text{cat}}$ ).

Since beam–background reactions dominate  $R_{\text{fus}}$  and 85% of fusion reactions are expected to occur inside the cathode, a simplified estimate of  $R_{\text{fus}}$  is given by substituting  $4\pi n_i v_i r^2 = I_{\text{man}} = I_{\text{meas}}/(1 + \delta_e)/(1 - \eta^2)$  into Eq. (1) and integrating to the cathode radius (note that  $\sigma_f$  is presumed to be constant inside the cathode):

$$R_{\text{fus}} \approx \int_0^{r_{\text{cat}}} \frac{I_{\text{man}}}{e} n_0 \sigma_f(-qV_{\text{cat}}) dr \approx \frac{I_{\text{meas}}}{e(1 + \delta_e)(1 - \eta^2)} n_0 \sigma_f(-qV_{\text{cat}}) r_{\text{cat}} \quad (5)$$

where the beam–cathode contribution ( $R_{\text{fus,cat}}$ ) in Eq. (1) is ignored. Equation (5) can be used for quick fusion rate estimates, but the full integral in Eq. (1) is evaluated when comparing this model with the experimentally measured neutron rates discussed below.

However, the reactivity estimate from this collisionless flow model underestimates the measured fusion production rate, and the expected linear increase of  $R_{\text{fus}}$  with neutral gas density is also not observed [4, 12]. Because of these shortcomings, a variety of hypotheses have been advanced to explain the observed behaviour of  $R_{\text{fus}}$  in these devices.

## 2.1. Multiple well structure in the core region

One hypothesis for the enhanced reactivity assumes that the ions are trapped in a virtual cathode structure near the core region. As the ions converge towards the centre of the device, their space charge forms a virtual anode, which is an electrostatic trap for electrons. In the same manner, cold electrons emitted from the cathode are thought to converge and form a virtual cathode inside the virtual anode. It is then suggested that this virtual cathode may trap energetic ions, resulting in an enhanced ion core density; since it is perfectly transparent, the ion lifetime in the energetic core region would be longer than that expected for ions flowing through the grids [4, 12, 13].

Some theoretical computations, assuming perfectly converging, collisionless and monoenergetic ion flows, predict such multiple well structures, but only virtual anodes are predicted from models including collisional and angular momentum effects [12, 15–17]. Measurements of the electrostatic potential distribution found virtual anodes, but no direct experimental evidence for a secondary virtual cathode has yet been observed. Neutron rates, X ray emission, and some electron orbit measurements were suggestive of multiple wells in early experiments, but no correlation was found between the formation of these structures and the resultant system reactivity [13, 14, 18, 4]. Indeed, the most recent experiments, which provide direct measurements of potential structures in the core region of a 5 keV SCIF device, showed only the single anode with no evidence of multiple well structure [14]. It is at low voltage (high permeance) where the ion space charge effects, important for the initial virtual anode formation, would be most prevalent.

## 2.2. Charge exchange effects

Charge exchange collisions remove the confined fast ions and replace them with cold (and much less reactive) ions. One would initially expect the system reactivity to be reduced because of this effect, but for some experiments, the fast neutral path length is as long or longer than the confined ion orbit length. Therefore, these collisions can then enhance the overall system fusion reaction rate.

A model of Hirsch's experiment that included the effects of charge exchange on the ion guns was developed by Baxter and Stuart [20]. It predicted neutron

rates and scalings with voltage, current and pressure comparable to Hirsch's observations, but to achieve agreement, the pressures used in the model were a factor of 20 higher than what Hirsch reported. However, the effects of recirculating ion current were ignored in the model, and it was shown experimentally that critical ion beam alignment, presumably to allow such recirculating currents, was necessary to achieve the highest reactivity [12].

For the gridded SCIF device employed here, the ions may recirculate many times through the high energy cathode region depending on the cathode transparency and neutral pressure. Previous measurements made at low pressure ( $\leq 50$  mPa), where the ion flow was essentially collisionless with respect to neutrals, indicated such a highly recycling ion flow [14]. However, in the higher pressure, glow discharge regimes studied by Miley et al., the ions do not recirculate but rather charge exchange on the first pass through the cathode [5]. Therefore, a more complete model, accounting for both charge exchange and a population of recirculating ions (if any), is necessary to describe the fusion reactivity in a SCIF device.

### 2.3. Beam-cathode contribution

For cathodes under energetic ion bombardment, a significant density of particles can become trapped in the material near the surface. These trapped atoms then can fuse upon collisions with incoming fast ions. This effect is used as the main source for the fusion reactivity of several commercial beam-target type neutron or fast particle sources [21, 22]. For the conditions under study here, the rate at which deuterium leaves the cathode surface is mainly limited by recombination. An approximation for the steady state surface density is given by equating the incident ion rate to the recombination rate at the surface or

$$\frac{I_f}{eA_{\text{cat}}} = K_r n_{\text{cat}}^2 \quad (6)$$

where  $I_f$  is the fast particle current,  $A_{\text{cat}}$  is the cathode surface area,  $K_r$  is the recombination rate constant and  $n_{\text{cat}}$  is the trapped fuel density. It has been found that  $K_r$  is a strong function of the material type, temperature and surface conditions (roughness, cleanliness, etc.), and for a particular material, the values of  $K_r$  are only known within 2 orders of magnitude [23]. It appears from Eq. (6) that  $n_{\text{cat}}$  is proportional to the square root of the ion current, but  $K_r$  is also a function of ion current (through the temperature dependence of the cathode on the ion current). These effects oppose each other, and the

resultant source density can be relatively independent of current.

To confirm this, an estimate of the cathode temperature is needed to estimate  $K_r$ . Assuming purely radiative heat transfer from the cathode of the input ion power, the cathode temperature  $T$  is given by

$$P = \frac{I_f V_{\text{cat}}}{A_{\text{cat}}} = \epsilon \sigma T^4 \quad (7)$$

where  $\epsilon$  is the emissivity of the cathode and  $\sigma$  is the Stefan-Boltzmann constant. The trapped fuel density can then be calculated using Eq. (6) with the appropriate value of  $K_r$  (see Section 5 for a specimen calculation). It was found that  $n_{\text{cat}}$  varies by less than a factor of 2 for values of  $I_f$  of interest here (between 10 and 150 mA). If conduction and convection were also considered, a lower cathode temperature would be expected and therefore a higher value of  $n_{\text{cat}}$ . However, the lowest order radiative model from Eq. (7) appears to be accurate experimentally, for the cathode would melt within 10% of the appropriate input power density.

Assuming a uniform fuel density within the effective penetration range for the energetic particles,  $\lambda$ , the fusion production rate contribution,  $R_{\text{fus,cat}}$ , is then given by

$$R_{\text{fus,cat}} = \frac{I_f n_{\text{cat}} \lambda [\sigma_{\text{fus}}(E)]}{e} \quad (8)$$

where the fusion cross-section is dependent on the cathode voltage,  $V_{\text{cat}}$  (e.g.,  $E \approx qV_{\text{cat}}$ ). Since  $n_{\text{cat}}$  is essentially independent of the cathode current,  $R_{\text{fus,cat}}$  is expected to scale linearly with injected current.

While similar current and voltage reactivity scalings are expected for all of the above models, they predict radically different spatial distributions of the fusion reactivity. The multiple well hypothesis predicts a highly localized source of reactivity near the origin of the system, the charge exchange model predicts a peaked but rather broad reactivity distribution and the beam-cathode contribution is localized at the cathode surface. In addition, the beam-cathode and charge exchange reactivity should be rather insensitive to the cathode grid spacing and transparency. In contrast, the multiple well model is very sensitive to the degree of focusing and the amount of recirculating current, and hence should depend strongly on cathode spacing and transparency.

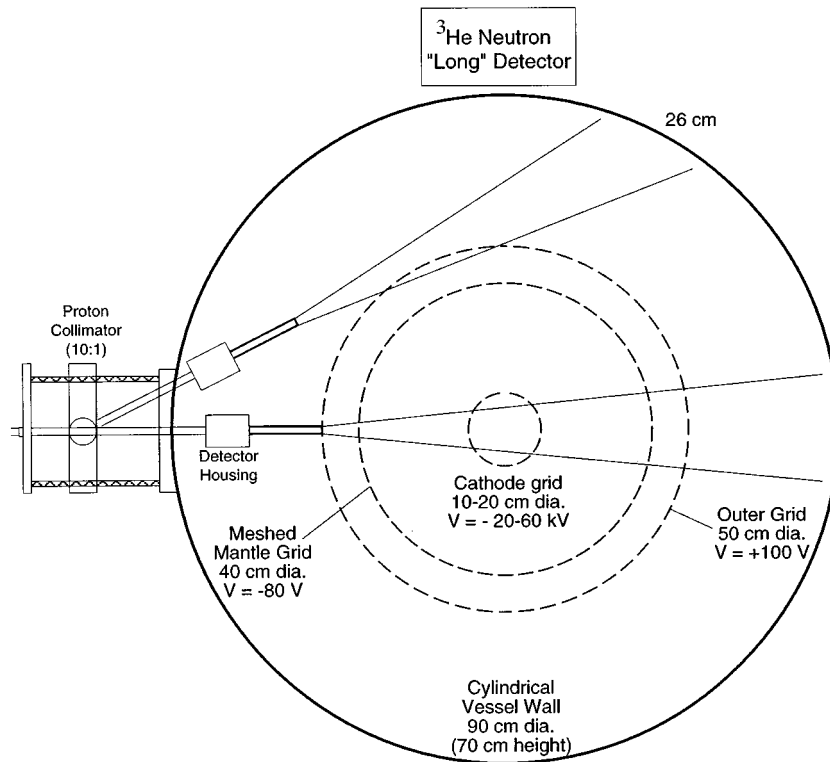


FIG. 1. Schematic top view of the WISCIF device, including the layout of the reactivity diagnostics. Typical operating voltages are listed with respect to the grounded vacuum chamber.

### 3. EXPERIMENTAL SETUP AND DIAGNOSTICS

The WISCIF experimental facility consists of three semitransparent spherical grids arranged concentrically in a cylindrical vacuum vessel (Fig. 1). A cold ( $T_e \sim 5$  eV,  $T_i$  is estimated to be  $\leq 0.1$  eV<sup>1</sup>) [14, 24], relatively uniform plasma provides a source of ions and is formed about the outermost grid. This grid (50 cm diameter) is biased positively to attract electrons generated by heated tungsten filaments. A fine mesh ( $\Delta x = 0.1$  cm  $< \lambda_{De}$ , the electron Debye length) covers the 40 cm diameter grid to electrostatically reflect these electrons away from the ion flow region, and permanent magnets are placed outside the vessel chamber to enhance the primary electron lifetime. Ions are then accelerated to fusion relevant energies by the semitransparent cathode grid ( $\eta = 0.85$ – $0.96$ ). The cathode current collected can be adjusted for fixed acceleration voltage by varying

the edge plasma density with the filament heating current or the outermost grid bias.

In order to produce a significant amount of fusion reactivity, the cathode is powered by a supply capable of 60 kV and 250 mA of steady state voltage and current, respectively. The cathode grid is supported by concentric tubes of quartz and alumina to provide the high voltage insulation and withstand the energetic plasma bombardment. The support lifetime is mainly limited by how quickly cathode material sputters onto the insulators, which may be a limitation for pushing the performance of these gridded systems to even higher currents and powers.

The total fusion neutron production rate is measured by a neutron counter similar to the one described by East and Walton [25]. These polyethylene shrouded <sup>3</sup>He detectors are rather insensitive to the incident neutron energy, allowing in situ calibration using a PuBe source. Measurement of the radial distribution of the fusion reactivity is provided by a collimated (0.79 sr) surface-barrier diode that is sensitive to the 3 MeV protons emanating from D–D fusion reactions. A design similar to that described by Nadler et al. [13] is employed, and the detector is

<sup>1</sup> The edge perpendicular temperature is estimated to be 0.1 eV for these calculations, which is a typical ion temperature for this type of glow discharge.

attached to a flexible bellows assembly, which allows the viewing angle to be varied during the experiment (Fig. 1). Thin aluminium (25  $\mu\text{m}$ ) and lead (13  $\mu\text{m}$ ) foils are placed at the opening of the collimator to shield the detector from plasma and X rays, while allowing the fusion protons to pass through. However, the combined thickness of the stainless steel collimator wall (1.3 mm) and the aluminium detector housing ensure that only protons that pass through the collimator are detected. The energy spectrum of the output signal is monitored with a multichannel analyser, and the proton signal is verified by operating at similar conditions in deuterium and hydrogen.

#### 4. DEUTERIUM–DEUTERIUM REACTIVITY MEASUREMENTS

##### 4.1. Cathode power and neutral background pressure scalings

To evaluate the suitability of these devices for applications, the dependence of the fusion reactivity on input power must be well understood. Observations of the systematic dependences of the fusion reactivity also provide insight into which sources of reactivity are dominant. For example, beam–beam reactions would scale as  $I_{\text{cat}}^2$  and with a different voltage and pressure dependence than beam–cathode or beam–background, which increase proportionally with  $I_{\text{cat}}$  (Eqs (1) and (5)).

Figure 2(a) presents a representative cathode voltage scan, which shows that the steady state system neutron production rate (NPR) scales simply with the energy dependence of the D–D fusion cross-section between 20 and 60 kV (indicated by the dashed curve); i.e.  $\text{NPR} \propto \sigma_{\text{fus,DD}}(E_i)$ , with  $E_i = V_{\text{cat}}$ . This observed scaling is consistent with past experiments performed in this voltage range at lower densities and power [1–5].

In Fig. 2(b), the NPR shows a linear dependence (indicated by the solid lines) on cathode current up to the maximum 250 mA for a variety of pressure ranges. The higher pressure discharges ( $P > 100$  mPa) are similar to the ‘star’ modes studied at lower density by Miley et al., where a self-sustaining, normal glow discharge forms [1–5]. A tight ion core and beamlets of light are observed as electrons are focused out of the cathode region by local asymmetries in the electrostatic potential. To operate at pressures below 100 mPa, the edge plasma source is required to sustain the ion flow, and a ‘converged core’ mode

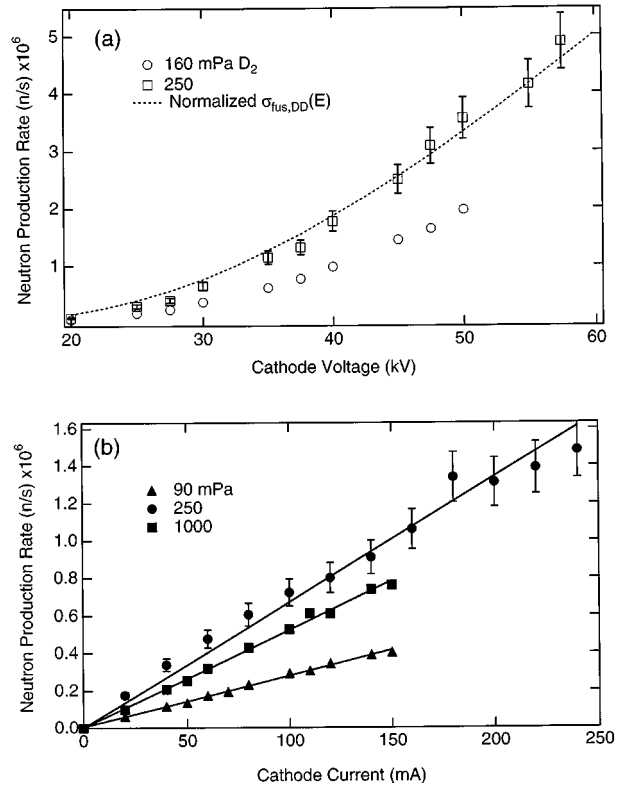


FIG. 2. Total NPR variations with (a)  $V_{\text{cat}}$  and (b)  $I_{\text{cat}}$  for the deuterium neutral pressures listed. For (a),  $r_{\text{cat}} = 5.0$  cm and  $I_{\text{cat}} = 20$  mA, and for (b),  $r_{\text{cat}} = 10.0$  cm and  $V_{\text{cat}} = 20$  kV.

persists [14]. The degree of core convergence is reduced as the pressure decreases, and the beamlets are no longer visible. While the discharge characteristics are different, the NPR is also found to scale linearly with current in this regime.

These cathode current and voltage scalings are consistent with the energetic particles fusing mainly with a background neutral density, as opposed to the counter-streaming beams fusing with each other. This is not unexpected, considering that the typical neutral densities ( $\sim 10^{19} \text{ m}^{-3}$ ) are much greater than the expected energetic ion densities ( $\sim 10^{15} \text{ m}^{-3}$ ).

Given these scalings, one might anticipate that as the neutral background density increases, the fusion rate would also increase proportionally (Eq. (5)). However, this is not seen experimentally, as shown in Fig. 2(b), where the 250 mPa case indicates a higher NPR than the 1000 mPa case. Figure 3 shows a composite pressure scan, where many NPRs from different operating cathode voltages and currents are compared by normalizing out their known dependences on the fusion cross-section and supply current. An increase in the normalized NPR is observed up until

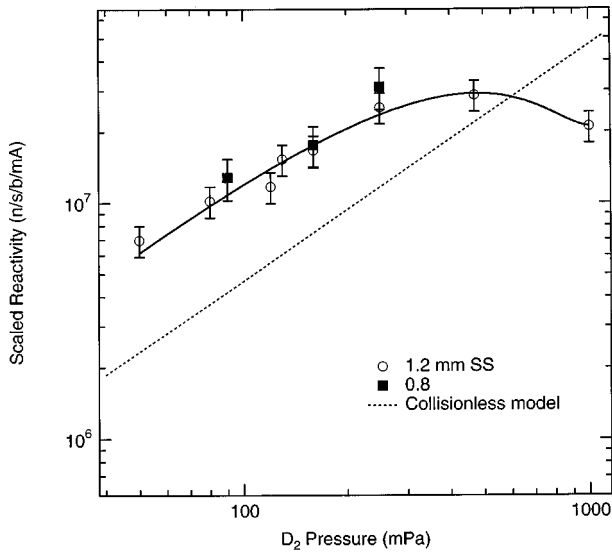


FIG. 3. Scaled neutron production rate ( $= \text{NPR}/\sigma_{\text{fus,DD}}/I_{\text{cat}}$ ) with pressure for two 5 cm radius cathodes with  $22.5^\circ$  wire spacing and different wire thicknesses (and hence different transparencies). Also included is the collisionless flow model estimate assuming  $\delta_e = 1$ ,  $\eta = 0.91$ .

about 300 mPa, after which a decline is indicated for higher pressures. This is qualitatively similar to the pressure scaling observed previously by Miley et al. in a smaller gridded device [4]. In contrast, Hirsch's experiment, which utilized ion guns instead of a distributed plasma source, found a monotonic increase in reactivity for decreasing pressure over a similar pressure range (10 to 1000 mPa) [12].

For comparison, estimates of the NPR expected from the simple collisionless flow model (Eq. (5)) are indicated by the dashed curve in Fig. 3. At the lower pressures studied, the measured NPR is a factor  $\sim 5$  greater than this ideal estimate, and the collisionless flow estimate does not reflect the observed pressure dependence in any way.

#### 4.2. Proton collimation results

As mentioned at the end of Section 2, the spatial distribution of the reactivity also provides a distinction between the various possible sources of fusion reactions. For example, if ions dominate the reactivity, a highly localized source near the origin would be expected. In contrast, a fast neutral background dominated system would have a far more diffuse, spatial distribution of reactivity.

Measurements of the fusion production spatial distribution are provided by the collimated proton detector, and the proton signal versus chordal height

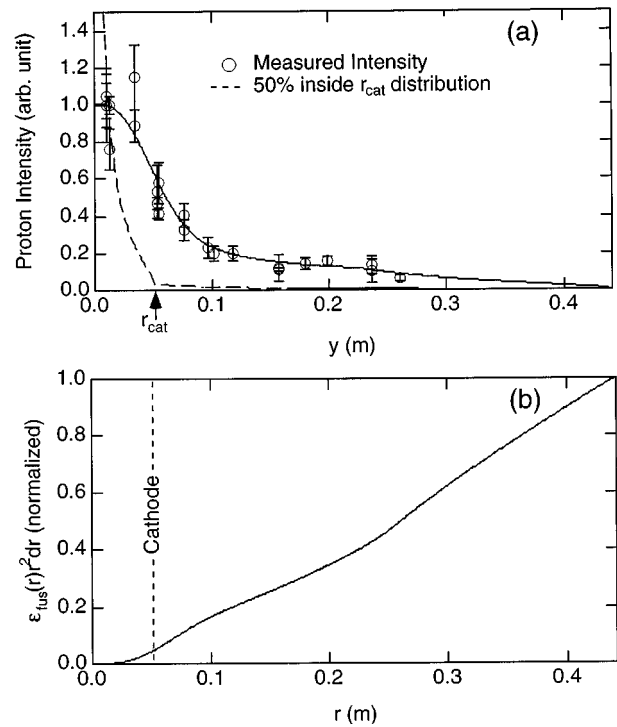


FIG. 4. (a) Line integrated proton intensity measurements and (b) the integral of the resulting Abel inverted radial reactivity profile,  $\epsilon_{\text{fus}}(r)$ . The dashed curve in (a) is the expected proton intensity distribution if 50% of the fusion production is generated inside the cathode ( $r_{\text{cat}} = 0.05$  m).

from the origin for a 35 kV, 20 mA discharge in 250 mPa of deuterium is shown in Fig. 4(a). While the proton signal intensity is peaked near the centre, it is important to note the detectable, non-zero signal observed outside the chordal height of 0.05 m, which is the cathode radius. This signal originating outside the cathode gives rise to most of the total fusion production, owing to the larger volumes at large radii.

The local reactivity,  $\epsilon_{\text{fus}}(r)$ , is derived from an Abel inversion [26] of the spline fitted data in Fig. 4(a), assuming that the chordally integrated reactivity decreases as  $1/r^2$  outside the outermost grid ( $r = 0.2$  m). This is equivalent to assuming that no source of fast ions or neutrals exists outside the outermost grid. While the exact form of  $\epsilon_{\text{fus}}(r)$  from the Abel inversion is fairly sensitive to the edge conditions assumed, the integrated system reactivity (shown in Fig. 4(b)) is not, especially inside the cathode region.

This is seen in Fig. 4(b), which shows the local reactivity,  $\epsilon_{\text{fus}}(r)$ , volume integrated to a given radius  $r$  as a function of  $r$ , to give the total reaction rate occurring inside  $r$ . It is apparent from Fig. 4(b) that

more than 90% of the total reaction rate originates outside the cathode radius of 5 cm. Hence, almost all of the fusion reactions are not produced in the converged ion core region but outside it, suggesting an extended, non-local source. To emphasize this point, Fig. 4(a) includes the shape of the curve expected from the proton collimation scan if only 50% of the integrated system reactivity is originating inside the cathode radius, much less inside the condensed ion core region ( $r_{\text{core}} \sim 1 \text{ cm} < r_{\text{cat}}$ ). The data clearly indicate a much broader radial distribution of the reactivity.

Another interesting feature shown in Fig. 4(a) is that the actual peak of the fusion reactivity may not occur at  $r = 0$ . The fusion proton signal at  $r = 0.04 \text{ m}$  appears to be slightly larger than that at  $r = 0$ . This is probably due to the formation of a slight virtual anode in the core region, which is formed by the converging ion beams there.

### 4.3. Cathode grid geometry scalings

In order to study the influence of flow convergence and the cathode geometry on the system fusion production, the cathode transparency, mesh spacing and

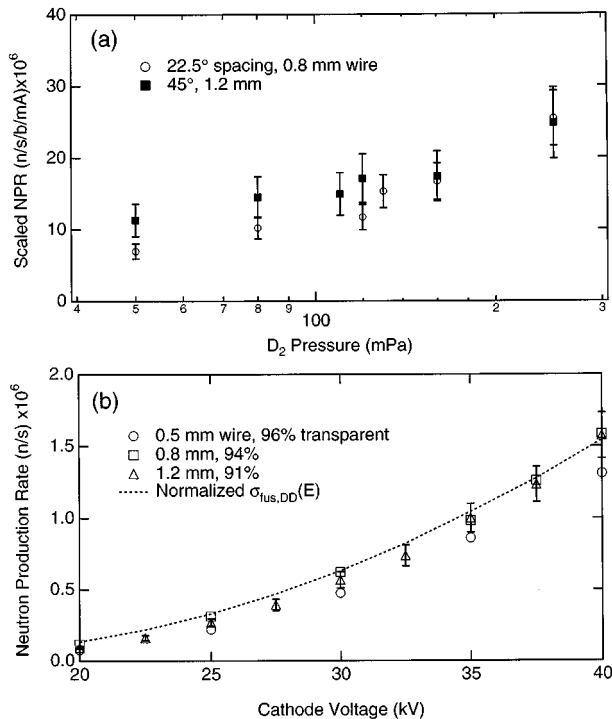


FIG. 5. Measured NPR for cathodes with (a) 91% transparency using 22.5 and 45° grid wire spacings and (b) varying cathode wire thicknesses, and hence transparencies, at 20 mA and 250 mPa for a 45° spacing grid.

size are varied. An increased mesh spacing results in a more defocused flow and hence a lower density core, as the asymmetries in the accelerating potential are larger [14]. This is expected to have little effect in beam-background dominated systems, unless the ion confinement time is somehow related to the flow convergence, as expected in the multiple well model. Decreasing the transparency of the cathode limits the ion lifetime of the system (assuming collisionless ion flow and losses only to the grid) and would be expected to significantly reduce the efficiency and fusion production of the system. By increasing the cathode size, the path length of the high energy region increases, and therefore an enhancement of the system fusion production may then be expected as well.

The effects of the cathode grid spacing on the NPR are shown in Fig. 5(a), where cathodes of comparable transparency but different wire spacings are included. These results indicate that no variation of the NPR is observed between cathodes with 22.5 and 45° grid spacings for pressures down to 50 mPa. Studies with 85% transparent grids similarly found no significant variation between cathodes of 15 and 22.5° spacings. However, earlier experiments found that the flow convergence does depend strongly on the cathode wire spacing [14]. Hence, it appears that the cathode geometry (or degree of flow convergence) has little effect on the overall system NPR.

By keeping the grid spacing (i.e. the total number of grid wires) constant, the transparency of the grid is varied by changing the diameter of the grid wires used. In Fig. 5(a), two different cathode wire thicknesses are compared, and between 50 and 250 mPa no significant difference is observed in the NPR for these two different cathodes. Figure 5(b) includes a related comparison at 250 mPa for a 45° spacing cathode, but with varying wire thickness and hence varying transparencies. No significant variation in the NPR is observed for changes in the grid transparency between 85 and 96%, where Eq. (5) (using Eq. (3)) predicts almost a factor of 3 difference in the expected NPR.

Variations in the cathode size do produce an observable variation; Fig. 6 includes a voltage scan at 250 mPa (20 mA cathode current), where grids of 2.5, 5 and 10 cm radius are compared ( $\eta = 0.91-0.92$ ). Little change is observed between the 2.5 and 5.0 cm cathodes, but a factor of  $\approx 1.5$  increase is measured between the 5 and 10 cm radius cathodes.

**Table I. Comparison of Various Collision Rates (in Units of  $s^{-1}$ ) in Different Regions of the Ion Flow for Typical Operating Parameters (35 kV, 20 mA,  $P = 130$  mPa) [27]**

(The effective ion cathode–collision rate is  $\sim 2 \times 10^6/s$  and the neutron production rate for these conditions is  $\sim 1 \times 10^6/s$ .)

Collision type	Edge ( $r > r_{\text{anode}}$ )	Acceleration ( $r_{\text{anode}} > r > r_{\text{cat}}$ )	Core/plateau ( $r_{\text{cat}} > r$ )
Charge exchange	$7 \times 10^3$	$3 \times 10^6$	$4 \times 10^6$
Neutral elastic scattering	$2 \times 10^5$	$10^5$	$10^5$
Ionization	$\sim 0$	$\sim 10^{-2}$	20
Ion–ion scattering	2	$7 \times 10^{-6}$	$4 \times 10^{-4}$

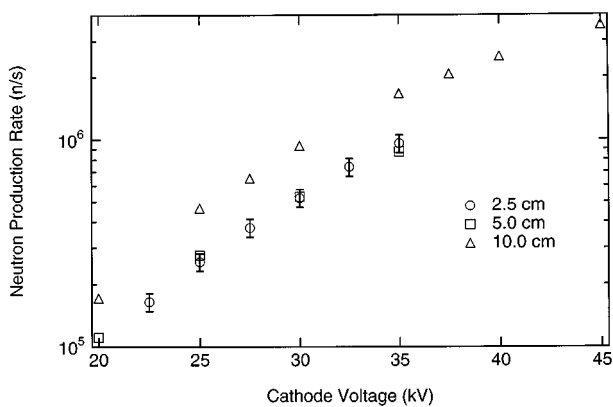


FIG. 6. Neutron production rate versus cathode voltage for  $r_{\text{cat}} = 2.5, 5.0$  and  $10.0$  cm for  $I_{\text{cat}} = 20$  mA and  $P = 250$  mPa.

#### 4.4. Cathode contribution to the system reactivity

The cathode grid itself, owing to the constant bombardment of energetic ions onto the wire surface with its trapped fuel density, is potentially a significant source of fusion production. To examine this possible source, a solid, 2.5 cm radius sphere and grids of different materials were installed as the high voltage cathode.

The solid cathode produced gradually increasing reactivity for decreasing pressure, as the NPR increased by at most a factor of 2 as  $P$  ranged from 1000 mPa down to 50 mPa. This is presumably due to the collisional degradation of the ion distribution from ion–neutral collisions. At the higher pressures, the solid target NPR is  $\leq 0.1$  of the total measured with the gridded system, indicating that beam–grid collisions constitute a relatively small

fraction of the NPR there. However, at the lowest pressure, the beam–sphere contribution is  $\sim 0.6$  of the total measured with the gridded system, and it can even surpass the values expected from the ideal, collisionless flow model.

Different cathode materials are also of interest, and the resultant NPRs of cathodes constructed of tungsten, titanium and stainless steel are included in Fig. 7. Each material has much different trapping properties and hence different values of  $K_r$  at lower temperatures. However, for the conditions studied, typical grid wire temperatures  $\sim 2000$  K are expected (Section 5), where all three materials have similar  $K_r$  properties [23]. Indeed, the data in Fig. 7 show little difference in the fusion rate between the various materials.

## 5. DISCUSSION

Measurements of the neutron count rate versus the neutral gas fill pressure indicate that ion–neutral collisions play a significant role in determining the system reactivity, and the dominant collisional process for the energy ranges considered is charge exchange. This is indicated in Table I, which compares the various relevant collision rates for different spatial regions in the ion flow for a typical WISCIF discharge [27]. Charge exchange is the dominant process in the high energy regions and even dominates over ion–cathode collisions at all but the lowest pressures.

The proton collimation measurements suggest the importance of the fast neutrals, since a significant amount of the fusion reactions are generated outside the cathode region. For a charge exchange dominated system, the cathode transparency or grid

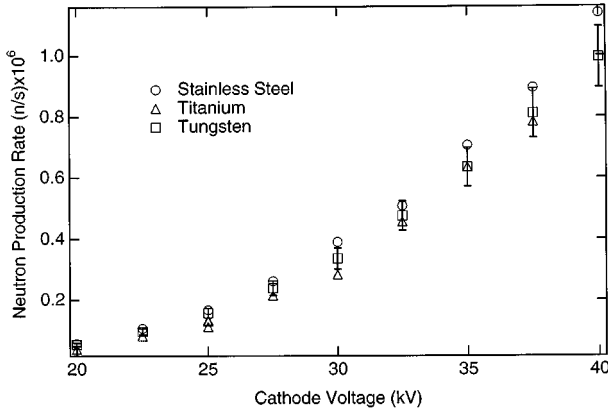


FIG. 7. Neutron production rate for cathodes of differing materials at 20 mA and 250 mPa. The 5.0 cm radius cathodes had a 45° spacing using 0.5 mm diameter wire.

spacing would not be expected to affect the system fusion production rate, since the resultant NPR is relatively unrelated to the condensed core plasma properties. Indeed, experimental measurements of the NPR for various materials, grid spacings and transparencies find no significant changes in the fusion production rate of the system.

A more complete fusion reactivity model for SCIF type devices would need to account for the contribution of the fast neutral background. To estimate this contribution for the WISCIF device, a classical fluid flow model calculation that accounts for charge exchange collisions is used. The number of fast ions removed from the ion flow via charge exchange as the flow evolves through the acceleration ( $r > r_{\text{cat}}$ ), plateau ( $r_{\text{cat}} > r > r_c$ ) and core regions is calculated from the ion fluid continuity equation (assuming steady state flow)

$$\begin{aligned} \nabla \cdot \frac{d\Gamma_i(r, E)}{dE} &= \frac{1}{r^2} \frac{d}{dr} \left( r^2 \frac{d\Gamma_i(r, E)}{dE} \right) \\ &= -n_0 \sigma_{\text{CX}}(E) \frac{d\Gamma_i(r, E)}{dE} \end{aligned} \quad (9)$$

where  $n_0$  is the neutral background gas density,  $d\Gamma_i(r, E)/dE$  is the differential radial ion flux as a function of radius and energy, and  $\sigma_{\text{CX}}(E)$  is the energy dependent charge exchange cross-section. The fast neutral flux ( $\Gamma_n$ ) is calculated similarly as

$$\frac{1}{r^2} \frac{d}{dr} [r^2 \Gamma_n(r, E)] = n_0 \sigma_{\text{CX}}(E) \Gamma_i(r, E) \quad (10)$$

and the source for thermal ions is given by

$$\begin{aligned} \frac{1}{r^2} \frac{d}{dr} [r^2 \Gamma_{\text{it}}(r)] \\ = \int_0^{E_{\text{max}}} dE n_0 [\sigma_{\text{CX}}(E) + \sigma_{\text{ii}}(E)] \frac{d\Gamma_i(r, E)}{dE} \end{aligned} \quad (11)$$

where  $E_{\text{max}}$  is the maximum energy of the ions at the particular radial location (i.e.  $E_{\text{max}} \approx -\Phi(r)$ ) and  $\sigma_{\text{ii}}(E)$  is the ion impact ionization cross-section. Electron impact ionization is also a source of thermal ions, but it provides less than a 1% overall effect on the system reactivity. This is due to the electrons having a lower ionization rate coefficient compared with the charge exchange and ion impact ionization rates at large radius ( $r \sim \rho$ ), where thermal ion production is most important [27]. Hence, only the fast neutral and ion distributions need to be considered to lowest order.

The electrostatic potential distribution for this model is taken to be a spherically symmetric, space charge limited potential distribution between the anode and the cathode, and a flat potential equal to the cathode bias is assumed inside the cathode radius to provide a best case estimate. A monoenergetic distribution of ion current is then injected at the edge of the potential well (0.2 m radius for the WISCIF device, i.e.  $d\Gamma_i(0.2, E)/dE = \Gamma_{i0} \delta(E - E_t)$ ), where  $E_t$  is the thermal energy of the ions at the edge and the incident ion flux,  $\Gamma_{i0}$ , is related to the cathode current collected in the experiment by

$$\Gamma_{i0} = \frac{I_{\text{meas}}}{4\pi e(1 + \delta_e)(0.2)^2(1 - \eta^2)} \quad (12)$$

where the  $1 - \eta^2$  term above accounts for the recirculating fraction of the ion flow (recall that  $\delta_e$  is the secondary electron emission coefficient for the cathode and  $\eta$  is the cathode transparency) [14]. The calculation follows the ion flow through the system by evaluating Eqs (9) to (11) for each energy group at each radial mesh location. Special attention is needed inside the cathode region to avoid divergence of the ion flux at the origin. Angular momentum will limit the degree of focusing of the ion flow towards the origin, and for the results described herein, the radial distribution is calculated using a Maxwellian distribution of transverse edge velocities and by then conserving the number of particles and the angular momentum. The mean radius of closest approach used was 1.0 cm, corresponding to the typical visible core size observed in these experiments [14, 28].

The fast neutrals from charge exchange are assumed to travel straight through to the vacuum chamber wall (0.45 m radius assumed), with the same degree of convergence as for the ions. The fusion rate can then be calculated from Eq. (1) using the resulting ion and fast neutral distributions.

Figure 8 shows the resulting uncollided fraction of ion current ( $= e\Gamma_i(r, E_{\text{max}})r^2$ ) after a single pass

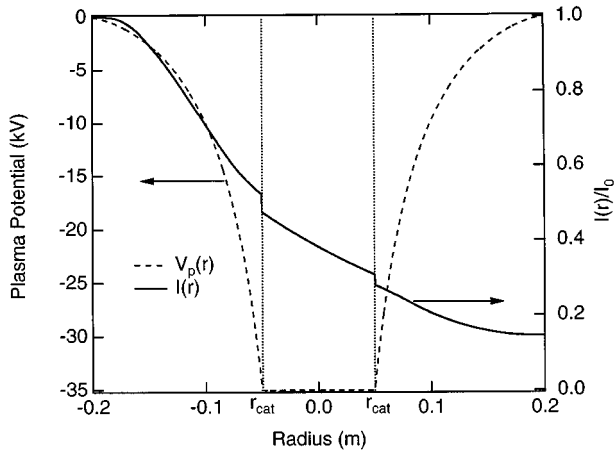


FIG. 8. Radial electrostatic potential distribution and the resulting uncollided fraction of ion current for a 35 kV discharge at 250 mPa of deuterium ( $\eta = 0.91$ ).

through the system for a 35 kV discharge at 250 mPa (for reference, the radial electrostatic potential distribution for the model is also included). The discontinuities in the ion current at  $r = \pm 0.05$  m signify the losses to the cathode grid (i.e. the ion and fast neutral densities are multiplied by the geometric cathode transparency,  $\eta = 0.91$  for this case). Charge exchange collisions clearly dominate under these conditions, for over 80% of the original ion distribution is converted to fast neutrals in a single pass.

Calculations of the fusion rate from the resulting ion and neutral distributions indicate that the ratio of fast neutral to ion induced fusion is approximately 2:1 for a fill pressure of 250 mPa. Therefore, the fast neutrals, theoretically, contribute at least twice as much reactivity as the ions at this pressure. The Abel inversion of the experimentally measured proton signal suggests that even more reactivity is generated outside the cathode (Fig. 4(b)).

The pressure scaling of the NPR predicted by this model is shown in Fig. 9 and is compared with the normalized measurements from a representative gridded cathode experiment. This plot also includes the data from the solid spherical target experiment for comparison (Section 4.4). Also for comparison, the values expected by the collisionless flow model (Section 2) are indicated by the dashed curve. A second model plot, where the solid cathode contribution is added to the charge exchange model reactivity, is included in Fig. 9 (thick curve) to provide an upper limit to the expected total NPR. This model accurately predicts the peak pressure, and the absolute value of the model NPR is also consistent with the observed values.

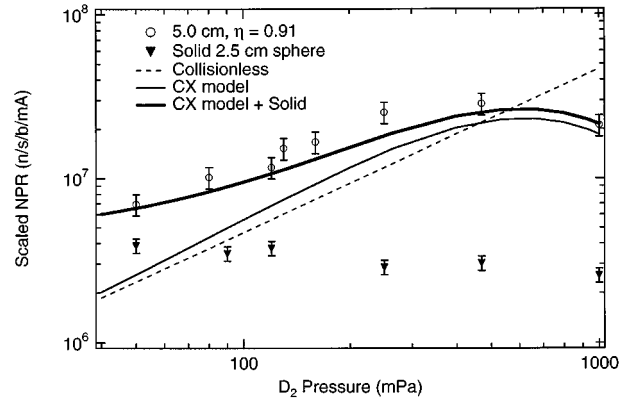


FIG. 9. Scaled NPR from the charge exchange fluid model versus pressure compared with gridded cathode measurements. Also included are the measurements from the solid cathode (2.5 cm radius) and the estimate from the collisionless flow model.

At the lowest pressures, the solid cathode contribution is needed to achieve agreement with the experimentally measured values. To estimate the amount of reactivity that can be reasonably expected from the cathode, the surface density of deuterium must be determined. Equation (6) indicates that this trapped density is strongly dependent on the cathode temperature through the dependence on  $K_r$ . The temperature  $T$  of the cathode sphere is estimated assuming a purely radiative loss of the ion input power (350 W). Estimating  $\epsilon = 0.35$ , the cathode temperature from Eq. (7) is  $\approx 1200$  K, and experimental measurements of  $K_r$  at 1000 K range between  $5 \times 10^{-31}$  and  $5 \times 10^{-27}$   $\text{m}^4/\text{s}$  [23, 29]. By taking the lowest value of  $K_r$ , an upper limit to the trapped cathode density is given, and by Eq. (6), this trapped density is  $4 \times 10^{24}$   $\text{m}^{-3}$  for the solid cathode studied (if  $\delta_e = 1$ , then  $I_f = 10$  mA). Assuming  $\lambda$  is  $\sim 1$   $\mu\text{m}$  and the fast particle current into the cathode is monoenergetic (in this case 35 kV), the beam-cathode contribution estimated from Eq. (8) is  $\approx 5 \times 10^4$   $\text{s}^{-1}$ . This is consistent with the measured value of  $\approx 10^5$   $\text{s}^{-1}$  when combined with the estimated reactivity from the beam-background reactions (also  $\approx 5 \times 10^4$   $\text{s}^{-1}$ ). Note that the fast neutrals can also collide with a trapped density of deuterium in the outer grids (also stainless steel) and the vacuum chamber wall (aluminium). However, the contributions of these sources are estimated to be less than 10 reactions/s for the above conditions and are therefore not significant compared with the cathode contribution.

Since the beam-cathode fusion production rate is a function of fast particle current (and not of

current density), the contribution for the semitransparent grids should be similar. However, the cathode area is different, and therefore the gridded cathodes operate at higher temperatures than the solid sphere (for like conditions). The resulting  $K_r$  constant would be higher, and therefore, the solid sphere estimate should provide an upper limit to the possible cathode contribution.

The observed size scaling of the NPR is also consistent with that of the charge exchange analysis, for while the fast neutral contribution would remain approximately constant for the three different cathode sizes studied (Fig. 6), the fast ion contribution is directly related to the cathode size. If the ratio of fast neutral to ion fusion is 2:1 for a 5 cm radius cathode at 250 mPa, then 33% of the system NPR is due to ions. By this analysis, a 33% improvement is expected for the 10 cm radius cathode ( $\sim 50\%$  is indicated), and only a 16% decrease is expected for the 2.5 cm radius cathode, where no noticeable difference is noted. While this does not completely explain the observed cathode size scaling, it is not entirely unexpected, given the experimental uncertainties, that the calculated distributions from the flow model are only approximate and that the effective fast neutral path length is not identical for the three cathodes.

While the overall NPR is consistent with that from this charge exchange model, details of the radial distribution of reactivity are not well reproduced, presumably owing to an insufficient model of the radial flow convergence in the central core region. The radial reactivity profile strongly depends on the exact shape of the potential inside the cathode. For example, a large virtual anode in the core region would shift the peak of the model reactivity profile away from the origin. As discussed earlier, the possible slight off-axis peak in the experimental proton collimation measurements is therefore consistent with a slight virtual anode in the core. However, the proton measurements also suggest that more reactivity originates inside the cathode region than that expected from the charge exchange analysis.

While the classical, charge exchange flow model successfully describes the reactivity observed in a gridded SCIF device, it does not completely account for the even higher fusion production rates reported originally by Hirsch [12] from the ion gun experiment. However, subsequent ion gun experiments [30] did not achieve the same performance as Hirsch, and the measured NPRs from these later investigations are in better agreement with the flow model predictions. The results from the gridded WISCIF experiments

also contradict those of the multiple well model, used as a possible explanation of the high reactivity of the ion gun experiments. The system reactivity in WISCIF does not depend strongly on flow convergence or transparency as expected from the multiple well model, and the proton collimation measurements show a more diffuse source of reactivity than would be expected from the multiple well model. Hirsch's results initiated much of the interest in SCIF type devices, and another experiment with ion guns would be useful in resolving these discrepancies between the different experiments.

Much higher injected currents will be needed to gain a significant beam-beam contribution to the fusion reactivity. A non-linear dependence of fusion reactivity on cathode current might then be observed. Owing to heat loads on the internal grids, such future experiments would most likely need to be performed in a short pulsed operation mode.

## 6. SUMMARY

Characterization of the various sources of reactivity and the influence of cathode power, ion-neutral collisions and cathode design have been investigated. The fusion production rate scales linearly with current, with the D-D fusion cross-section with voltage, and as expected with pressure considering the effects of charge exchange on the fusible ion flow distribution. Proton collimation experiments verify that the diffuse fast neutral population provides most of the observed fusion production, especially for the glow discharge modes ( $P > 100$  mPa). The system NPR does not depend strongly on the cathode material, wire spacing or transparency, and the cathode grid itself may contribute significantly to the measured NPR, especially at low pressures ( $\leq 100$  mPa).

These results are inconsistent with the expectations from the multiple well model or any other model invoking a centralized source of reactivity. Although the measured NPRs exceed the collisionless estimate at low pressure, the reactivity can be accounted for if the beam-cathode and fast neutral contributions are considered. It appears that no anomalous trapping of ions is required to explain the observed fusion reactivity scalings for these systems.

## ACKNOWLEDGEMENTS

The authors would like to thank R. Ashley for his technical assistance and N. Hershkowitz, R. Hirsch,

G. Kulcinski, G. Miley, R. Nebel, W. Nevins, G. Poe, J. Santarius and L. Wainwright for useful discussions and for their contributions to this project. This work was supported, in part, by the Electric Power Research Institute under agreement No. 6424-51010 and the College of Engineering, University of Wisconsin.

## REFERENCES

- [1] NADLER, J.H., MILEY, G.H., GU, Y., HOCHBERG, T., *Fusion Technol.* **21** (1992) 1639.
- [2] MILEY, G.H., et al., in *Proc. 3rd Conf. on Dense Z-Pinches*, London, 1994, AIP Conf. Proc. **299** (1994) 675.
- [3] ANDERL, R.A., et al., in *Fusion Engineering (Proc. 16th Symp. Champaign, 1995)*, IEEE, New York (1995) 1482.
- [4] MILEY, G.H., et al., *Fusion Technol.* **19** (1991) 840.
- [5] NADLER, J.H., MILEY, G.H., GU, Y., HOCHBERG, T., *Fusion Technol.* **20** (1991) 850.
- [6] BUSSARD, R.W., *Fusion Technol.* **19** (1991) 273.
- [7] KRALL, N.A., *Fusion Technol.* **22** (1992) 42.
- [8] BARNES, D.C., NEBEL, R.A., TURNER, L., *Phys. Fluids B* **5** (1993) 3227.
- [9] NEVINS, W.M., *Phys. Plasmas* **2** (1995) 3804.
- [10] RIDER, T.H., *Phys. Plasmas* **2** (1995) 1853.
- [11] LAVRENT'EV, O.A., *Ann. N.Y. Acad. Sci.* **251** (1975) 152.
- [12] HIRSCH, R., *J. Appl. Phys.* **38** (1967) 4522.
- [13] NADLER, J.H., GU, Y., MILEY, G.H., *Rev. Sci. Instrum.* **63** (1992) 4810.
- [14] THORSON, T.A., DURST, R.D., FONCK, R.J., WAINWRIGHT, L.P., *Phys. Plasmas* **4** (1997) 4.
- [15] DOLAN, T.J., VERDEYEN, J.T., MEEKER, D.J., CHERRINGTON, B.E., *J. Appl. Phys.* **43** (1972) 1590.
- [16] BLACK, W.M., KLEVANS, E.H., *J. Appl. Phys.* **45** (1974) 2502.
- [17] CHERRINGTON, B.E., VERDEYEN, J.T., SWANSON, D.A., *Ann. N.Y. Acad. Sci.* **251** (1975) 139.
- [18] VERDEYEN, J.T., CHERRINGTON, B.E., SWANSON, D.A., MEEKER, D.J., *Ann. N.Y. Acad. Sci.* **251** (1975) 126.
- [19] BLACK, W.M., ROBINSON, J.W., *J. Appl. Phys.* **45** (1974) 2497.
- [20] BAXTER, D.C., STUART, G.W., *J. Appl. Phys.* **53** (1982) 4597.
- [21] KIM, J., *Nucl. Instrum. Methods* **145** (1977) 9.
- [22] BARSCHALL, H.H., in *Neutron Sources for Basic Physics and Applications (CIERJACKS, S., Ed.)*, Pergamon Press, Oxford (1983) 57.
- [23] WILSON, K.L., in *Data Compendium for Plasma-Surface Interactions, Nuclear Fusion Special Issue*, IAEA, Vienna (1984) 28.
- [24] CHAPMAN, B., *Glow Discharge Processes*, Wiley, New York (1980) 52.
- [25] EAST, L.V., WALTON, R.B., *Nucl. Instrum. Methods* **72** (1969) 161.
- [26] MIYAMOTO, K., *Plasma Physics for Nuclear Fusion*, MIT Press, Cambridge, MA (1987) 507.
- [27] JANEV, R.K., LANGER, W.D., EVANS, K., Jr., POST, D.E., Jr., *Elementary Processes in Hydrogen-Helium Plasmas*, Springer-Verlag, Berlin (1987).
- [28] THORSON, T.A., *Ion Flow and Fusion Reactivity Characterization of a Spherically Convergent Ion Focus*, PhD Thesis, Univ. of Wisconsin-Madison, Madison, WI (1996) 22.
- [29] LIDE, D.R. (Ed.), *Handbook of Chemistry and Physics*, 71st edn, CRC Press, Boca Raton, FL (1990) 10-282.
- [30] GARDNER, A.L., HATCH, D.M., CHAN, A.I.Y., EVANS, R.P., *Ann. N.Y. Acad. Sci.* **251** (1975) 179.

(Manuscript received: 17 July 1997)

Final manuscript accepted: 16 December 1997)

E-mail address of T.A. Thorson:  
thorson@uwmfe.neep.wisc.edu

Subject classification: N0, Ie